Characterization of optical coatings by photothermal deflection

Mireille Commandré and Pierre Roche

An overview of photothermal deflection principles and applications is given. The modeling of temperature distribution and the calculation of deflection that is due to both the refractive-index gradient and the thermal deformation of the sample are presented. Three configurations usually employed are compared, and their respective advantages are discussed in relation to their application. The calibration for absolute measurement of absorption is detailed, showing that calibration limits the accuracy of measurement. Some examples of specific information obtained by photothermal mapping of absorption are given. © 1996 Optical Society of America

Key words: Optical coatings, photothermal deflection, calibration, absorption, local defects.

1. Introduction

Optical absorption is responsible for decreases of reflectance and transmittance values for dielectric thin-film optical components and then acts as a limiting factor for optical performances but also causes reduced values of the radiation damage threshold.[1–3] Indeed, absorbed radiative energy is converted to heat that propagates through the sample, and the induced temperature change can lead to damage. Radiation damage resistance has been shown to be dependent on both absorption losses and thermophysical properties of materials, especially the thermal conductivity.[4–6] Furthermore, substantial progress has been made in thin-film technology during past few years, and classical values of losses are now in the 10^{-6}–10^{-4} range. However, the determination of losses by measurement of reflectance (R) and transmittance (T) is limited to $1 - R - T > 10^{-3}$. Under these conditions, an accurate characterization of absorption and thermal properties of optical thin films has become an important task for the improvement of optical performances and a better understanding of damage mechanisms.

The authors are with the Laboratoire d'Optique des Surfaces et des Couches Minces, Unité Associée au Centre National de la Recherche Scientifique, Ecole Nationale Supérieure de Physique de Marseille, Domaine Universitaire de St. Jérôme, 13397 Marseille Cedex 20, France.

Received 20 November 1995; revised manuscript received 4 March 1996.

0003-6935/96/255021-14$10.00/0

Photothermal deflection (PD) techniques were developed at the beginning of the 1980's[7–9] and have been widely employed since to characterize optical coatings.[3,10–25] The basic process of photothermal methods is measuring the heating of the sample caused by optical absorption. In PD, the heated domain is probed by a laser beam that is deflected. Because of the order of magnitude of thermal effects, all the photothermal methods require a time-dependent excitation light. Each technique can be used in both modulated or pulsed modes. Resulting from the optical absorption of the intensity-modulated (or pulsed) pump beam, a local temperature rise occurs and a thermal wave propagates in the structure. This modulated (or pulsed) temperature rise is accompanied by spatial refractive-index variations and a buckling of the sample surface that is due to thermal expansion. PD lies in measuring the deflection of the probe beam, which is due to the refractive-index gradients and to the thermal buckling of the sample surface. Obviously amplitude and phase of the PD signal depend on both the optical absorption and thermal properties of the thin film. At a low modulation frequency, one can obtain the absorptance value on the conditions that a proper calibration has been performed and frequency or temporal response can give information about thermal properties (diffusivity or thermal conductivity).

Furthermore, PD is a direct measurement of absorbed energy; thereby the photothermal signal is linear over a large range of absorbed optical power and is vanishing when there is no absorption. PD is also insensitive to scattered light, at least the external part. The success of PD originates from various

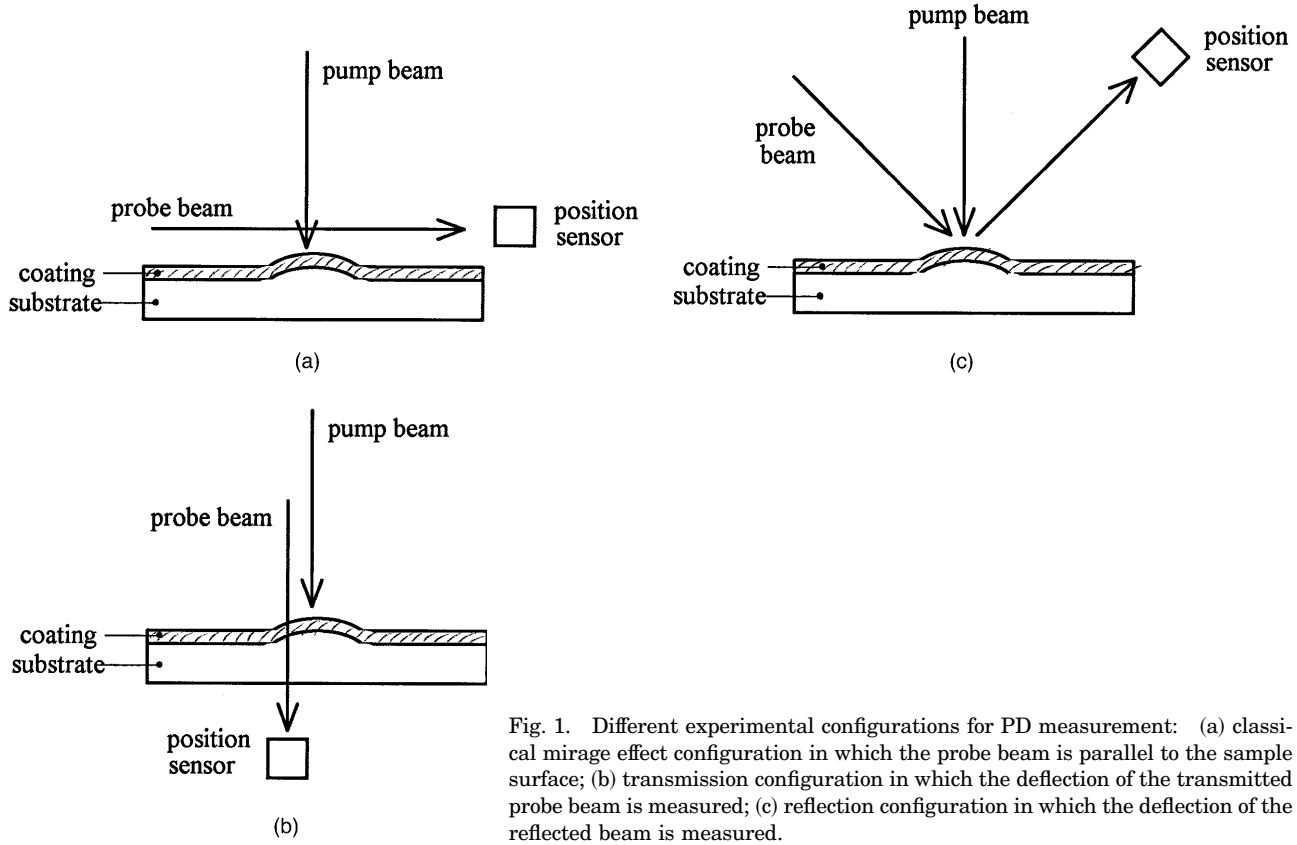

Fig. 1. Different experimental configurations for PD measurement: (a) classical mirage effect configuration in which the probe beam is parallel to the sample surface; (b) transmission configuration in which the deflection of the transmitted probe beam is measured; (c) reflection configuration in which the deflection of the reflected beam is measured.

other advantages: the absence of any mechanical contact with the sample (PD is a nondestructive method) and the ease of implementing (no sample preparation, for example). For absorption measurement, the greatest advantages are high sensitivity and the possible application to spectroscopy and above all to high spatial resolution imaging.

In this paper we present an overview of three configurations (defined by the relative positions of the probe beam and the sample) that have been used for implementing this technique and their applications. This overview does not give complete insight into the great variety of the photothermal methods that can be used, but we have selected these three schemes because they can be carried out with exactly the same experimental setup and they are complementary. We present a short survey of the modeling of temperature distribution and the calculation of PD that is due to the refractive-index gradient as well as to the thermal buckling of the sample. The orders of magnitude of these two components are compared in the different configurations. We take a special interest in showing the advantages of each configuration, depending on the application.

PD permits accurate measurements of very small absorption losses as low as 10^{-6}. We describe an experimental setup realized in our laboratory for absorption mapping. Calibration is an important task that is detailed. Absorption mapping has been shown to be a complementary tool for the characterization of the cleanness and optical quality of bare substrates,[18–20] and some results are presented.

2. Photothermal Deflection Principles and Applications

In Fig. 1 we present three schemes that have been used for implementing this technique. Figure 1(a) is the classical mirage effect or transverse configuration: The probe beam is in the air, parallel to the sample surface and is deflected by the index gradient in air in the direction normal to the surface. Below we call the scheme given in Fig. 1(b) the transmission configuration (also called the collinear configuration): The probe beam goes through the sample and is deflected by both the radial index gradient in the three media and the surface displacement. We refer to the scheme given in Fig. 1(c) as the reflection configuration: The deflection of the reflected probe beam is measured and originates from the index gradient in the air and in the coating and from the thermal expansion of the surface.

Some variants can be used: For example, in the reflection configuration, the probe beam can be directed to the sample back surface and propagate in the substrate. Or in the mirage effect, the probe beam can go through the sample under the surface (polished lateral faces are then required for the substrate).

A. Modeling of Photothermal Deflection

The calculation of PD can be divided into two parts. First, by using the expression of heat source resulting

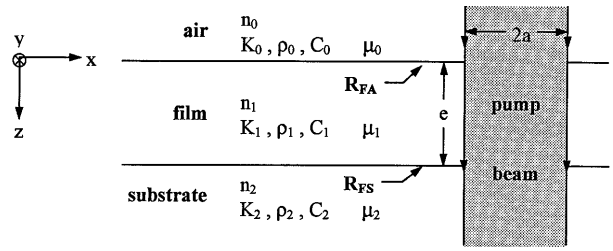

Fig. 2. Definition of notation used in the text: n_i and k_i are the real and the imaginary parts of the complex index of medium i, respectively ($i = 0$ to 2), K_i is the thermal conductivity of medium i, ρ_i is the mass density of medium i, C_i is the heat capacity per unit mass of medium i, ν is the modulation frequency, $\omega = 2\pi\nu$ is the modulation pulsation of the pump beam, μ_i is the thermal diffusion length of medium i defined by $\mu_i = (K_i/\rho_i C_i \pi\nu)^{1/2}$, R_{FA} and R_{FS} are the thermal resistances at the air–film and film–substrate interfaces, respectively, e is the film thickness, and $2a$ is the diameter at $1/e^2$ of the Gaussian pump beam.

from optical absorption in the coating, we calculate the modulated temperature distribution in the three media, air, coating, and substrate. Then the effects of temperature distribution on the probe-beam propagation can be calculated. The notation of different parameters is given in Fig. 2. The air and the substrate are assumed to be transparent and semi-infinite. The film is infinite in both the x and the y directions. The pump beam is normal to the sample surface and is assumed to be Gaussian.

1. Calculation of Modulated Temperature

We denote as $T_i(x, y, z, t)$ the time-dependent component of temperature distribution in medium i. The calculation of the steady temperature rise can be found in Ref. 26. The three media are assumed to be isotropic, so the temperature distribution keeps a cylindrical symmetry $T_i(r, z, t)$ where $r^2 = x^2 + y^2$, as for the pump beam. In this paper we are interested in only harmonic solutions: $T_i(r, z, t) = T_i(r, z) \exp(j\omega t)$. The equations governing the thermal phenomena are considered with the assumption that heat transfer is due only to thermal conduction: Radiation losses and natural convection are negligible at ambient temperature.[27] Furthermore, temperature distribution is assumed to be unaffected by the thermal buckling of the sample.[8,9]

Under these conditions, temperature distribution in the three media satisfies the equations of heat diffusion[8]:

$$\nabla^2 T_0(r, z, t) - \frac{\rho_0 C_0}{K_0} \frac{\partial T_0}{\partial t} = 0, \tag{1}$$

$$\nabla^2 T_1(r, z, t) - \frac{\rho_1 C_1}{K_1} \frac{\partial T_1}{\partial t} = \frac{-Q_1(r, z, t)}{K_1}, \tag{2}$$

$$\nabla^2 T_2(r, z, t) - \frac{\rho_2 C_2}{K_2} \frac{\partial T_2}{\partial t} = 0, \tag{3}$$

with the following conditions at the boundaries $z = 0$ and $z = e$:

$$T_0(z = 0) = T_1(z = 0) - R_{FA}\Phi_{F\to A}, \tag{4}$$

$$T_1(z = e) = T_2(z = e) + R_{FS}\Phi_{F\to S}, \tag{5}$$

$$\Phi_{F\to S} = -K_1\left(\frac{\partial T_1}{\partial z}\right)_{z=e} = -K_2\left(\frac{\partial T_2}{\partial z}\right)_{z=e}, \tag{6}$$

$$\Phi_{F\to A} = K_0\left(\frac{\partial T_0}{\partial z}\right)_{z=0} = K_1\left(\frac{\partial T_1}{\partial z}\right)_{z=0}. \tag{7}$$

Relations (4) and (5) are the equations of continuity for the temperature (taking into account the thermal resistance at the interfaces), and relations (6) and (7) are the equations of continuity for the heat flows.

$Q_1(r, z, t)$ is the heat source resulting from the optical absorption in the film, and $\Phi_{F\to A}$ and $\Phi_{F\to S}$ are the heat flows from the film toward the air and the substrate.

If we take into account the interference effects in the film, the expression of the heat term is

$$Q_1(r, z, t) = \frac{4\pi k_1}{\lambda} \frac{n_1}{n_0} \frac{P_0}{\pi a^2} \exp(-2r^2/a^2) \times \exp(j\omega t) \left|\frac{E_1(z)}{E_0}\right|^2, \tag{8}$$

where P_0 is the incident power of the pump beam, a is the $1/e^2$ radius of the pump beam, and E_i is the electric field in the medium i ($i = 0, 1$). $|E_1/E_0|^2$ is a sinusoidal function of z, with a period of $\lambda/2$.

We can note that, in the low modulation frequency range, the thermal diffusion length [defined by $\mu_i = (K_i/\rho_i C_i \pi\nu)^{1/2}$] of the film is higher than its thickness ($e < \mu_1$, thermally thin film). In this case the variation of the heat source with z can be ignored, and a mean-energy approximation is valuable for calculating the temperature distribution in the three media.

These equations can be solved with the radial Fourier transform:

$$T_i(r, z) = 2\pi \int_0^\infty \sigma J_0(2\pi\sigma r) \tilde{T}_i(\sigma, z) d\sigma, \qquad (i = 0 \text{ to } 2), \tag{9}$$

where J_0 is the Bessel function of the order of 0.

Some general statements can be made about the form of the solutions. The temperature rise in the three media is always proportional to the incident power of the pump beam P_0 and to the extinction coefficient k_1 of the film. The thermal conductivity of the film K_1 appears at different places in expressions of temperature rises; this parameter plays an important part in the temperature distribution.

To gain physical insight into thermal wave propagation, we present in Fig. 3 the calculated isotherms in the three media for two modulation frequencies (50 and 5000 Hz) in the case of a classical single-layer film of extinction coefficient $k_1 = 10^{-4}$ deposited on a

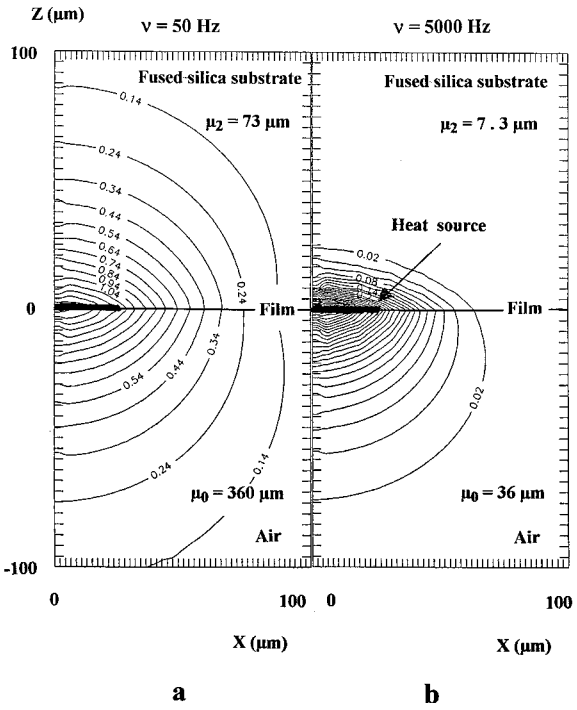

Fig. 3. Modulated temperature distribution in the three media: isotherms calculated with classical values of thermal parameters for the film ($e = 0.5$ μm, $k_1 = 10^{-4}$, $K_1 = 0.1$ W/mK, fused-silica substrate, $P_0 = 1$ W, $a = 25$ μm): (a) $\nu = 50$ Hz, (b) $\nu = 5000$ Hz.

fused-silica substrate. The value of the thermal diffusion length is given in each case for substrate and air. Physically the thermal diffusion length is the distance over which the amplitude of a planar harmonic thermal wave decays exponentially to $1/e$ of its initial value. For low modulation frequency (Fig. 3a) the thermal diffusion length in the two media is larger than the radius at $1/e^2$ of the pump beam: The temperature rise (the values are given for the isotherms in degrees Celsius) extends in the x, y plane beyond the pump-beam profile. For high modulation frequency (Fig. 3b) the thermal diffusion length decreases: The heated domain is reduced and nearly coincides with the illuminated domain in the radial direction.

The different refractive-index gradients that are probed in the different configurations of PD can be easily seen. The radial gradient associated with the energetic profile of the pump beam is probed in the transmission configuration, whereas the gradient in the direction perpendicular to the sample surface is probed in the transverse one.

2. *Photothermal Deflection that is due to the Refractive-Index Gradient*

We neglect the effect of the acoustic wave that accompanies the temperature rise. The measured deflections are generally very small, lower than 10^{-5} rad; the total shift of the probe beam is lower than 0.1 μm, which is small compared with the probe-beam diameter (≈40 μm). Under these conditions, if the probe beam propagates in the Z direction, the deflection in the Y direction is given[8] for the medium i by

$$\theta_{Y,i} = \frac{1}{n_i}\frac{\partial n_i}{\partial T}\int_{\text{path } i} \mathrm{d}Z\left[\frac{\partial T_i}{\partial Y}(X, Y, Z, t)\right]_{X=X_0,Y=Y_0}, \quad (10)$$

where (X_0, Y_0) is the position of the probe-beam center in the plane $Z = 0$ and $\partial n_i/\partial T$ is the temperature coefficient of the refractive index of medium i.

The PD is always linearly related to the incident power of the pump beam and to the extinction coefficient of the film.

In Refs. 8, 18, and 25 one can find some examples of the calculation of deflection versus relative positions of pump- and probe-beam centers for transmission configuration and versus distance between sample surface and probe-beam center for a mirage effect.

For the transmission configuration, the total deflection is the sum of complex deflections in the three media: air, film, and substrate. The deflection in the substrate is generally predominant.[18] The deflection inside the film is proportional to $1/n_1\,\partial n_1/\partial T$, and it is generally small for thin films ($e \leq 1$ μm). But we can remark that, concerning values of $1/n_1\,\partial n_1/\partial T$, only some data can be found in publications,[28] and the sign and the absolute value of this parameter are different from the bulk ones. The sign plays an important role because it changes the phase of the deflection in the film.

3. *Calculation of Deflection that is due to Thermal Displacement*

For the transmission and the reflection configurations, there are two contributions to PD: index gradients and thermal expansion of the surfaces. The calculation of the deflection that is due to the thermoelastic deformation of the sample surface has been developed in Refs. 9 and 29. The rigorous calculation involves solving the Navier–Stokes equations:

$$(1 - 2\nu_i)\nabla^2\mathbf{u} + \nabla(\nabla\cdot\mathbf{u}) = 2(1 + \nu_i)\alpha_i\nabla T \qquad (i = 1, 2),$$

where $\mathbf{u}$ is the displacement vector, ν_i is the Poisson ratio, and α_i is the thermal expansion coefficient of medium i. Only approximate analytic solutions are available. If the probe beam propagates in the Z direction, the deflection in the Y direction is given by

$$\theta_Y \approx 2\frac{\partial u_z}{\partial Y}(X_0, Y_0, Z = 0) + 2\frac{\partial u_z}{\partial Y}(X_0, Y_0, Z = e)$$

for the reflection configuration and by

$$\theta_Y \approx (n_1 - n_0)\frac{\partial u_z}{\partial Y}(X_0, Y_0, Z = 0) + (n_2 - n_1)\frac{\partial u_z}{\partial Y}(X_0, Y_0, Z = e)$$

for the transmission configuration, where (X_0, Y_0) is the position of the probe-beam center in the plane $Z = 0$. The first term in these equations corresponds to the deflection at the air–film interface and the second

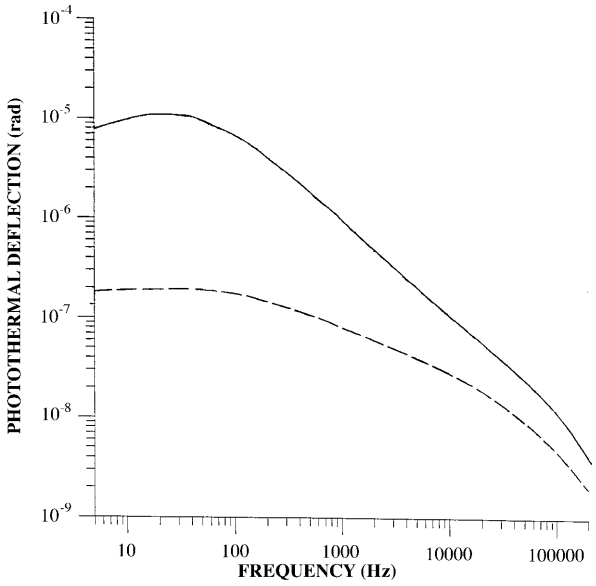

Fig. 4. Components of PD that is due to the refractive-index gradient (dashed curve) and to thermoelastic deformation (solid curve), calculated in the reflection configuration for classical values of parameters (e = 0.5 μm, BK7 substrate), versus modulation frequency.

one to the deflection at the film–substrate interface. The thermal deformations of the film and the substrate contribute together to the total deflection. One shows that each deflection is proportional to the considered thermal expansion coefficient.

Comparative calculations of the two contributions, index gradient and thermal displacement, show that for the transmission configuration the total deflection that is due to index gradients is higher than the deflection that is due to thermal expansion. It is the opposite for the reflection arrangement. In Fig. 4 we give a comparative calculation of the two deflections in the reflection configuration versus modulation frequency. The values of thermal, optical, and geometric parameters are classical values for a high-index film deposited on a BK7 substrate. We can see that the modulus of the deflection decreases when the frequency increases, whatever the origin of the deflection.

B. Applications

We can distinguish between two kinds of application, those related to the determination of thermal parameters and those related to the study of absorption characteristics. In the three configurations, the variation of PD, particularly the phase versus the modulation frequency, can be used to determine the thermal properties of optical thin films.[17] With regard to absorption measurement, the possibilities of PD are various. It can be used for spectroscopic measurement (no problem of photodetector response), and it allows absorption mapping[18–20] and microscopy.[10,11,16] Furthermore, because measurement time can be short, PD can be used to follow evolution versus time of thin-film absorption. So photoinduced changes have been observed[14] in some oxides in thin-film form. PD has also be applied to the discrimination between film and substrate absorption.[24] It can be implemented in vacuum, for example, for thin-film deposition study. In our laboratory we also use PD for measuring the attenuation during guided propagation.[23] Simultaneous measurements of absorption and attenuation allow us to reach an accurate balance of energy losses.[22,23]

Three general remarks can be made concerning the advantages and disadvantages of the different configurations. First, if we consider the number of thermal or physical parameters of the film involved in PD, we find four parameters for the mirage effect: $\rho_1 C_1$, the heat capacity per unit volume; K_1, the thermal conductivity; R_{FS}, the thermal resistance at the film–substrate interface; and e, the thickness of the film. For each reflection (R) and transmission (T) configuration we have to add another parameter: α_1, the thermal expansion coefficient for the R configuration and $1/n_1\ \partial n_1/\partial T$, the relative temperature coefficient of refractive index for the T configuration. This can be interesting if one wants to determine this last parameter, but in the general case it can complicate the task as, for example, the determination of thermal conductivity or the calibration of PD for absorption measurement (see Subsection 3.B).

The second remark is that in the mirage effect the PD depends strongly on the distance between the probe-beam center and the sample surface and is nearly independent of the diameter of the pump beam. On the contrary, in the R and T configurations, the PD signal increases greatly when the pump beam is tightly focused. This effect originates from the fact that in these configurations we detect the radial temperature gradient that is approximately proportional to the slope of the Gaussian curve of the pump beam.[9] A consequence is that for pump-beam diameters lower than 100 μm and at low modulation frequencies, the detectivity of R and T configurations is higher than that of the mirage effect. These two techniques are well suited for high spatial resolution absorption imaging.

Last, in R and T configurations, the PD depends on the relative position of pump and probe beams in the x, y plane and presents a maximum that is generally chosen as the measurement position. This property makes the beam alignment easier and can be used to control the positioning and repositioning of samples, which is important for absorption mapping (see Section 4 on absorption mappings before and after cleaning or coating). In fact, the R and T configurations are similar, and the choice between the two techniques is generally determined by experimental considerations such as the optical design and spectral properties of the component to be measured or the bulk absorption of the substrate. Indeed the T configuration is more sensitive to the bulk absorption in the substrate because the probe beam goes through the sample in the directly heated substrate.

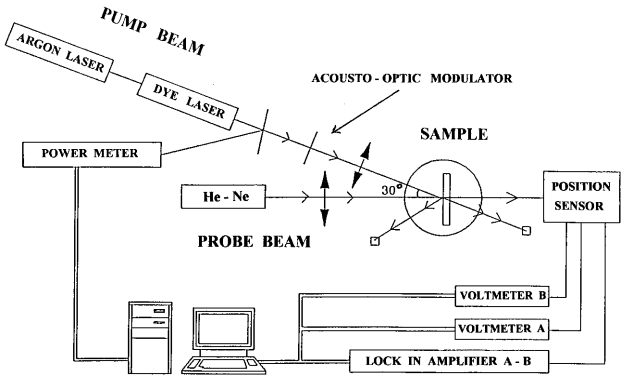

Fig. 5. PD experimental setup in the transmission configuration.

3. Experimental Procedure for Absorption Mapping

A. Experimental Setup

The layout of the experimental setup in the transmission configuration is shown in Fig. 5. The pump-beam laser can be a cw argon laser (in particular, 514.5-nm line) or a cw dye laser (spectral range 570–640 nm for rhodamine 6G dye). This beam is directed so that the angle of incidence on the sample surface will be approximately 30° with respect to the normal with s polarization. It is modulated by an acousto-optic modulator at a frequency of 27 Hz. A power meter measures the pump-beam power. The incident power on the sample is ~100 mW. The probe laser is a 0.8-mW helium–neon laser (633 nm) that is normal to the sample surface. The pump and the probe beams are focused onto the front surface of the sample: The beam diameters at this point are ~100 μm for the pump beam and 40 μm for the probe beam (diameter at $1/e^2$). The relative position of the two beams on the sample surface is adjusted in order to find maximum probe-beam deflection. A quadrant position sensor is utilized to measure the deflection of the probe beam that is transmitted by the sample. The output signal of the sensor is directed to the differential input of a two-phase lock-in analyzer. The sample is mounted on an x–y translation stage that enables it to move in both directions parallel to the sample surface. Accordingly we can map the absorption variations at different points on the sample surface. The sample positioning is reproducible with a precision of a few micrometers.

Because the PD is governed not only by the optical absorption but also by the conversion of radiative energy to heat and by the thermal diffusion, any spatial inhomogeneity of thermophysical constants of thin film (density, thermal conductivity, diffusivity) can modify the photothermal signal. The evaluation of spatial resolution for absorption measurement is complicated by thermal effects.[9] Indeed we use a low modulation frequency for absorption measurement, and we have seen that in this frequency range the heated domain extends in the x, y plane beyond the illuminated domain. If thin-film thermal properties are homogeneous, the spatial resolution is limited mainly by the size of the illuminated region, which is 100 μm in our experimental conditions. The increment step is 50 μm. The studied surface is generally 550 μm × 750 μm (165 points). Further results of absorptance are given in ppm (1 ppm = 10^{-6}).

After calibration the lowest absorptance that we can detect is 10^{-6} with an incident power of ~100 mW, which corresponds, for example, to an extinction coefficient of some 10^{-7} for a TiO_2 film of 250-nm thickness.

B. Calibration for Absolute Measurement of Absorptance

Obtaining the absolute value of the absorptance of a coating requires a calibration of the PD, by a comparison with samples of known absorption. We have seen that the PD depends not only on the absorption but also on the optical, thermal, and geometric parameters of the substrate and of the film. Any comparison between two different samples supposes that, in the considered measuring conditions, the two compared samples have similar geometric and thermal properties, or at least that these properties have little influence on PD. Of course, calibration samples have to be made with the same substrates as those of the samples under investigation. However, for materials in thin-film form, it has been pointed out that especially the thermal conductivity, the thermal resistances at the interfaces, the thermal expansion coefficient, and the thermal coefficient of the refractive index vary with the coating material, the deposition technique, and the film thickness.[5,28,30–32] Furthermore, the values of these parameters for a film are different from those of bulk material: thermal conductivity, for example, is 1 or 2 orders of magnitude lower in a film than in bulk. Generally we lack numerical values for all these parameters.

1. *Influence of Film Properties on the PD/A Ratio*

We can calculate the influence of thin-film properties on PD or on the ratio of the PD to the absorption. The calculations below of PD that is due to index gradients are performed for the transmission configuration. It is shown that, in their possible variation range, ρ_1, C_1, and R_{FS} have little influence on PD but that this influence increases with modulation frequency.

In Fig. 6 we give a calculation of the normalized PD versus film thermal conductivity for film thicknesses of 0.05 and 0.5 μm. Classical values of K_1 found in publications are close to 10^{-1} W/m K and some values are in the 10^{-2} to 10^{-1} range.[5,32] By comparing Figs. 6a and 6b, we can see that the influence of K_1 is higher for thick films and for films with low thermal conductivity ($<10^{-1}$ W/m K). If we compare two films of the same thickness but of different values of K_1, then the error for absolute measurement of absorption is lower than 2% for H films (where H represents a quarter-wave layer, $e \approx 0.05$ μm in the visible range) (Fig. 6a) but can be ~18% for 10H films (Fig. 6b, $e \approx 0.5$ μm). We can remark that for all calculated points of Figs. 6a and 6b, the thermal diffusion length of the film remains higher than its

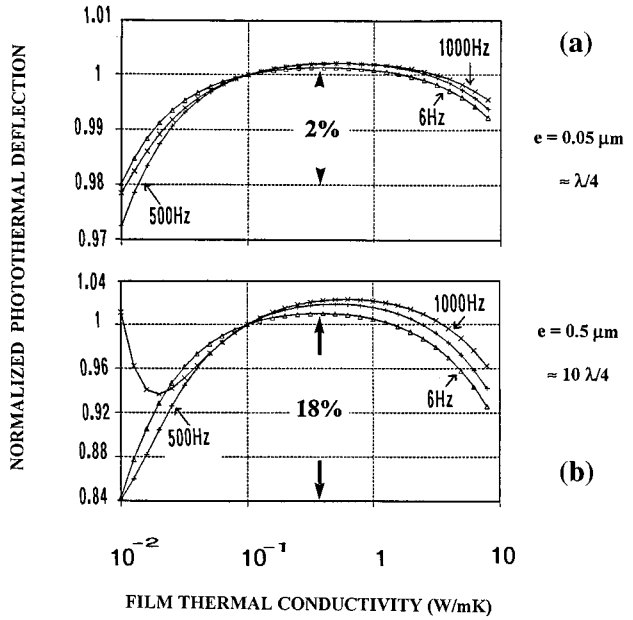

Fig. 6. Influence of thermal conductivity of thin film on total PD (which is due to index gradients) in the transmission configuration for modulation frequencies of 6, 500, and 1000 Hz: (a) for a film of thickness $e = 0.05$ μm (≈λ/4 for a high-index film), (b) for a film of thickness $e = 0.5$ μm (≈10 λ/4).

thickness (at $\nu = 6$ Hz, μ_1 varies from 23 to 728 μm when K_1 varies from 10^{-2} to 10 W/m K).

In Fig. 7 we present a calculation of the normalized ratio PD/A versus film thickness. When the thickness varies from 0.1 μm (2H film) to 1 μm (20H film), the relative variation of the PD/A ratio is ~10%. Important variations occur for films thicker than 1 μm. This behavior originates from the fact that for thick films the deflection inside the film increases and significantly contributes to the total deflection. If we compare two films with thicknesses of 1 and 5 μm, even at $\nu = 6$ Hz, the error can be 80%. This result shows that it is difficult to compare films of different thicknesses, particularly when $e \geq 1$ μm.

The influence of $1/n_1\ \partial n_1/\partial T$ on PD is plotted in Fig. 8 for a film with a thickness of 0.5 μm (10H film).

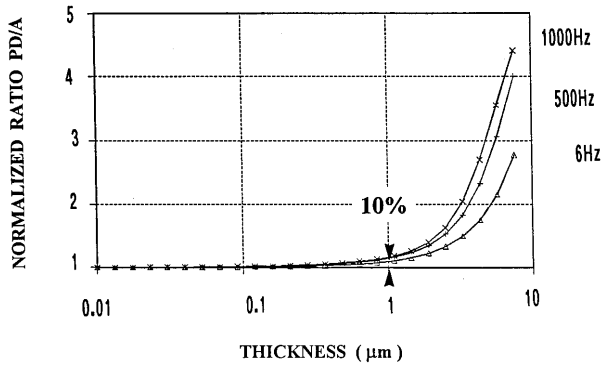

Fig. 7. Influence of film thickness on total PD in the transmission configuration for modulation frequencies of 6, 500, and 1000 Hz ($K_1 = 0.1$ W/m K).

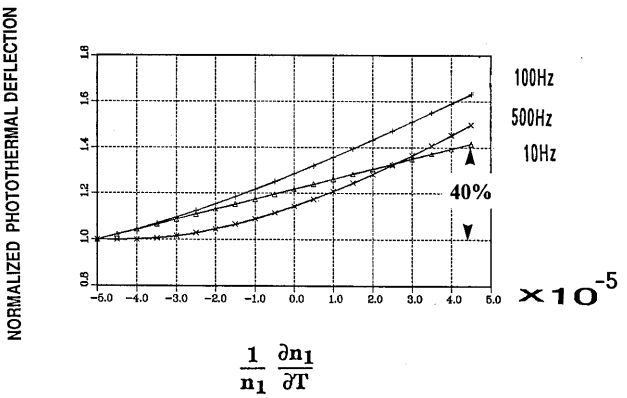

Fig. 8. Influence of the temperature coefficient of the refractive index of the film on total PD in the transmission configuration for modulation frequencies of 10, 500, and 1000 Hz ($e = 0.5$ μm, $K_1 = 0.1$ W/m K).

Even at $\nu = 10$ Hz, when films of different values of $1/n_1\ \partial n_1/\partial T$ are compared, the error can be 40%. This effect originates from the high absolute values of $1/n_1\ \partial n_1/\partial T$ for thin films: The deflection in the film contributes to the total deflection even for thin films. Obviously the error increases with film thickness.

Calculations of Figs. 6–8 show that thermal conductivity, film thickness, and $1/n_1\ \partial n_1/\partial T$ have a nonnegligible part in the PD/A ratio. In conclusion we can say that it is possible to perform an accurate calibration of PD. But for this purpose, it is necessary, first, to use low modulation frequency, and second, to use calibration samples similar to the studied samples: same substrate, same coating material, and thickness of the same order of magnitude. These conditions have to be carried out more especially as the film is thick. When they are fulfilled, the calibration problem is reduced to a simple determination of the constant of proportionality, which is called the calibration coefficient. This calibration coefficient must be checked for each kind of sample under characterization.

Similar calculations can be carried out for the reflection configuration. The thermal expansion coefficient of the film plays the same part as $1/n_1\ \partial n_1/\partial T$ does for the transmission configuration. For thick films, the film deformation significantly contributes to the PD. With regard to calibration, the mirage effect is the best configuration because only two film parameters (e and K_1) have an effect on PD.

2. *Calibration Procedure*

The principle of our calibration is to compare the photothermal signal with the losses measured by a classical spectrophotometer, $A \approx 1 - R - T$, assuming that scattering losses are negligible (scattering losses can also be controlled separately). The detectivity of R and T measurements is limited to approximately some 10^{-3}; thus the calibration samples have to be highly absorbing (a few 10^{-2} at least). To obtain such highly absorbing films, we deposit oxides by using reduced O_2 partial pressure. Because spectro-

Table 1. Comparison among Absorptances Measured by PD and by[33] LM for Four SiO_2 Films of Increasing Thicknesses

Optical Thickness	Absorptance ($\times 10^{-4}$) Measured by PD[a]	Absorptance ($\times 10^{-4}$) Measured by LM[b]	Ratio		
			Simple Ratio	Corrected Ratio $\times \lambda_2/\lambda_1$ $1/\cos i_{film}$	
$\lambda_2/4$	1.0 ± 0.2 $\sigma = 1.1$	1.4	1.40	1.28	≈ 1.3
$\lambda_2/2$	2.1 ± 0.4 $\sigma = 0.23$	3	1.43	1.30	
$3\lambda_2/4$	2.2 ± 0.4 $\sigma = 0.6$	3	1.36	1.24	
λ_2	3.4 ± 0.7 $\sigma = 0.2$	5	1.47	1.34	
Bare substrate (fused silica)	0.28 ± 0.06 $\sigma = 0.2$				

[a] $\lambda_1 = 600$ nm, $i_{air} = 30°$, s polarization.
[b] $\lambda_2 = 514.5$ nm, normal incidence.

photometric and photothermal measurements have a different spatial resolution, we compare the mean values of absorptance on the same 3 mm × 3 mm area.

The accuracy of absolute measurement of absorption by PD is limited by the calibration. When various calibration samples with similar characteristics are used, the dispersion of measured calibration coefficients is ~20% when the relative uncertainty of the photothermal signal is some percent only.[18]

3. Comparison among Measurements by Laser Microcalorimetry and Photothermal Deflection

To evaluate the accuracy of our calibration, we have performed comparative measurements of the same low absorbing samples by laser microcalorimetry (LM) and PD. We have measured eight samples provided by V. Scheuer from Technische Hochschule Darmstadt[33]: four SiO_2 films and four Ta_2O_5 films deposited on fused-silica substrates by ion-beam sputtering. LM measurements were performed at Darmstadt.

Results concerning SiO_2 samples are gathered in Table 1. The optical thicknesses of the layers are $\lambda/4$, $\lambda/2$, $3\lambda/4$, and λ for $\lambda = 514.5$ nm. The PD and the LM measurements were performed under different experimental conditions: wavelength 600 nm, incidence angle 30°, and s polarization for PD, and wavelength 514.5 nm and normal incidence for LM. In the case of SiO_2 deposited on fused silica, we can neglect the interference effect within the film, and we can compare the absorptances directly: $A = 4\pi k_1 e/(\lambda \cos i)$, where i is the incidence angle in the film. The ratio LM/PD can be easily corrected to take into account the different illumination conditions of the two measurements (we neglect the dispersion of the extinction coefficient). The corrected ratio is close to 1.3 for all SiO_2 samples, although the film thickness is different. The deviation between LM and PD is ~30%, which is of the same order of magnitude as the dispersion of our calibrations.

In Table 2 we give the results for Ta_2O_5 samples. Because the PD and the LM measurements are not performed under the same illumination conditions, it is not possible to compare the measured absorptances directly. But from refractive index and thickness determined by spectrophotometric measurements and from absorptance measured by PD, we can calculate absorptance under the LM illumination conditions. The ratio LM/PD is then close to 1.8 for all Ta_2O_5 samples, which is different enough from the ratio measured for SiO_2 samples. To calibrate the PD, we have used the same calibration sample (a TiO_2 layer on a fused-silica substrate) for all the films (SiO_2 and Ta_2O_5), which can explain the different values of the LM/PD ratio. Furthermore, the dispersion of extinction coefficient probably has to be taken into consideration.

Table 2. Comparison among Absorption Measured by PD and by[33] LM for Four Ta_2O_5 Films of Increasing Thicknesses

Optical Thickness	Spectrophotometry		PD		LM	Ratio	
	$n_1(\lambda_1)$	e(nm)	A ($\times 10^{-5}$) Measured for λ_1[a]	A ($\times 10^{-5}$) Calculated for λ_2[b]	A ($\times 10^{-5}$) Measured for λ_2[b]		
$\lambda_2/4$	2.113	50.2	4.9	5.1	9.3	1.82	≈ 1.8
$\lambda_2/2$	2.113	114.7	6.6	9.0	15.0	1.67	
$3\lambda_2/4$	2.117	162.5	5.7	5.5	10.0	1.82	
λ_2	2.113	238.9	7.1	11.0	20.0	1.82	

[a] $\lambda_1 = 600$ nm, $i_{air} = 30°$, s polarization.
[b] $\lambda_2 = 514.5$ nm, normal incidence.

These comparisons confirm our above conclusions: PD allows an accurate comparison among similar samples, but absolute determination of absorption is less precise. Calibration is the weak side of PD used to measure absorption. This study was carried out on single-layer films, but the results can be applied to multilayer components. First, the thickness of a multilayer stack is often higher than 1 μm. Furthermore, one can have thermal resistances at each interface. For these reasons it is necessary to be more careful in the determination of the calibration factor for multilayer components. Fortunately PD is well suited for imaging absorption, and for this application knowing the absolute value of absorptance with a high accuracy is not necessary. We see below that absorption mapping can provide specific information on glass surfaces and optical coatings.

4. Photothermal Mapping of Absorption: Specific Information

The usually employed techniques of characterization of polished surfaces, bare and coated, are Nomarski microscopy, scattering measurements,[34] mechanical profilometry, and total internal reflection microscopy.[35,36] They give information about roughness and local defects. As for the PD technique, it yields absorption data.

The surface quality of bare substrates and preparation procedures take on an important role in optical coating performances. For this reason PD has been used for mapping absorption of fused silica and multicomponent glass substrates.[18–20] Measurements have shown the existence of highly nonuniform absorption localized at the substrate surface. High absorption sites can be 20 times as absorbing as the mean value, but we can find areas with very low absorption ($\approx 10^{-6}$). Typically for fused-silica substrates, the mean value of surface absorption is approximately 8×10^{-6}. Chemical analyses (see, for example, Refs. 37–39) have shown contamination that is due to impurities and residues from polishing compounds and cleaning solvents (metals, CeO_2 or ZrO_2, organic solvents, H_2O). Such absorbing residues are likely to be responsible for the measured surface absorption.

A. Comparison with Nomarski Microscopy and Scattering Mapping

Nomarski microscopy is the most commonly used method for inspecting the optical quality of substrates before coating. Absorption mappings of bare substrates have been compared with Nomarski microscope photographs and scattering mappings of exactly the same area. For this purpose we have measured, on the same samples and with the same spatial resolution, scattered light simultaneously with PD. Each sample has been observed through the Nomarski microscope; the photographic field is the same one as for absorption and scattering mappings.

Thus we first find no systematic correlation between Nomarski photography and absorption mapping. The difference in lateral spatial resolution for the two techniques, some micrometers for Nomarski microscope and 100 μm for the photothermal setup, makes it difficult to interpret the images. Nevertheless we can observe some features:

- Generally very large defects seen through the microscope (>10 μm) are present in the photothermal image and induce high absorption;
- We find some large defects (for example, local peeling) visible through the microscope as well as in scattering mapping, which lead to no significant variation of absorption;
- A substrate that presents an empty field through the microscope can be associated with significant variations of absorption on photothermal mapping. This nonuniform absorption can be caused by the presence of absorptive impurities (residues from the polishing compounds and cleaning solvents, particulate contamination occurring after polishing and cleaning, for example) on the surface. So photothermal mapping appears to be a complementary tool for the characterization of cleanness and optical quality of bare substrates.

Similarly we find no systematic correlation between scattering and absorption mappings. The spatial resolution is the same now. Scattering mapping tests mainly surface profile and refractive-index variations whereas photothermal mapping gives us extinction coefficient variations. Hence it is not surprising that these two images are different. In Fig. 9 we present the absorption [Fig. 9(a)] and the scattering [Fig. 9(b)] mappings measured on the same area of a T3 polished[40] BK7 substrate. We can see a defect that absorbs but does not scatter and another one that scatters but does not absorb. The mean value of surface absorptance is 80 ppm and the mean value of total integrated scattering is 20 ppm: all the losses are 100 ppm. Indeed, the behavior of surface defects depends on their nature. Some defects induce scattering and absorption simultaneously. But it is possible to find scattering but nonabsorbing defects as well as absorbing and nonscattering defects (Fig. 9).

Thus the photothermal mapping of absorption gives specific information on the surface contamination of bare substrates. Accurate absorption measurements are a valuable tool for better preparation of surfaces before coating in order to obtain very low-loss components.

B. Influence of Polishing and Cleaning on the Absorption of Surfaces

It is well known that glass surfaces have chemical compositions generally very different from bulk compositions; the methods used to create the surface, the grinding and polishing processes, the cleaning procedure, and the storage conditions modify the surface composition. This is the result of different complex phenomena such as adsorption–desorption processes, diffusion, nonstoichiometry, phase separation,

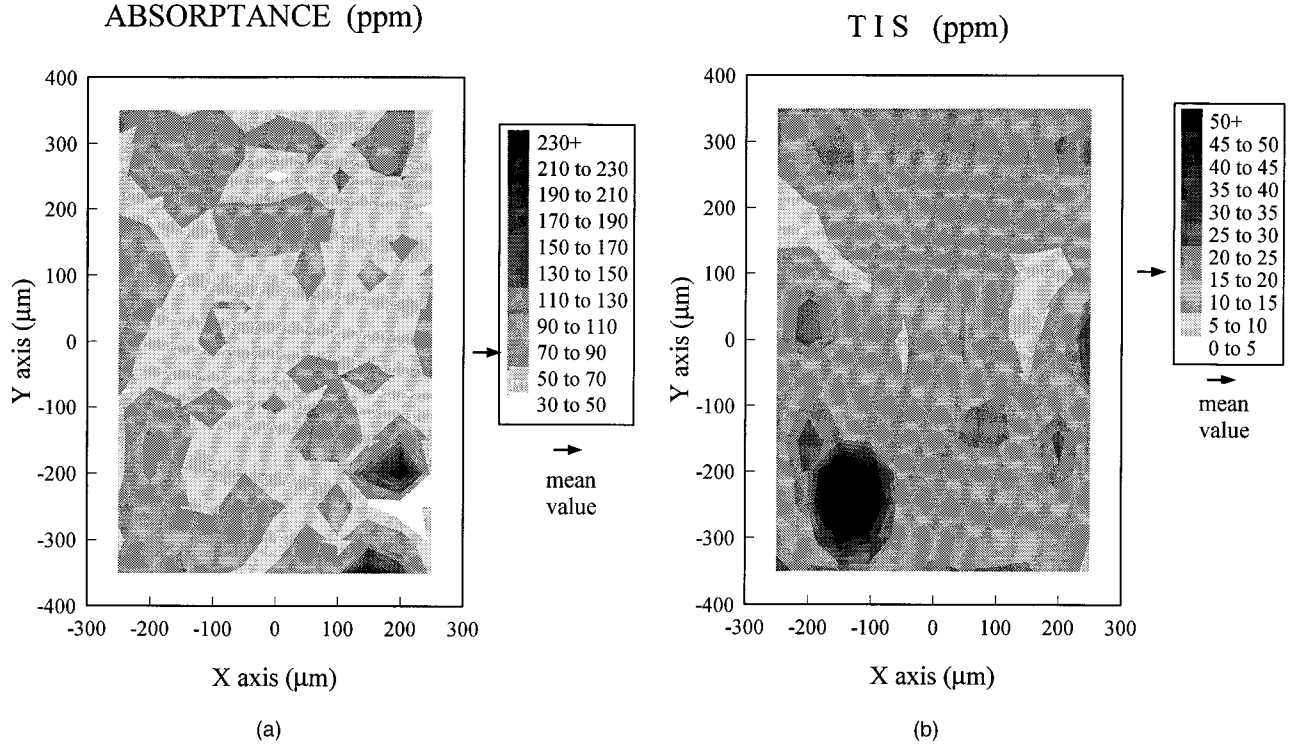

Fig. 9. Simultaneous mappings of (a) absorption, (b) total integrated scattering (TIS) on the same area (500 μm × 700 μm) on a BK7 bare substrate: a defect can scatter but not absorb and vice versa.

and segregation effects. In these considerations, we must distinguish between single and multicomponent materials: The latter generally have a more complex behavior. In alkali glasses (such as BK7), migration of metallic ions, especially Na, to the surface has been observed.[41–43] The thickness of such surface layers with modified composition can reach 1 μm, depending on the type of glass and the nature and duration of the treatment.

Absorption mapping can give interesting information about these surface phenomena. If a sample is simply kept in a dry and clean environment, the absorption mappings recorded on this sample at long intervals (some days) remain identical. However, any cleaning operation changes the absorption mapping. It is interesting to compare the mappings of the same sample before cleaning (as received from the supplier) and after cleaning: These mappings are hardly ever correlated. Figure 10 shows absorption mappings of the same area on a BK7 substrate (T3 polished[40]) before and after cleaning through a conventional procedure in an automatic cleaning apparatus. The spatial distribution of absorption is completely modified by cleaning, whereas the average surface absorptance decreases from 54 to 40 ppm. In Table 3 we give mean surface absorptance values before and after cleaning for some BK7 and fused-silica substrates (T3 polished[40]). Generally the first cleaning reduces mean surface absorptance.

These effects are valuable for all tested materials; they show that the contaminants that cause surface absorption are not tightly bound to the substrate surface; generally the cleaning processes used seem to displace absorbing impurities without completely removing them.

We now see that the behavior of a surface in terms of absorption depends on polishing quality and substrate material. Two sets of fused-silica substrates fabricated with the same material but polished under different conditions have been cleaned successively with increasingly effective procedures: soft manual cleaning then automatic cleaning. Examples of results are given in Fig. 11. The main conclusion is that the levels of mean surface absorptance of commercial grade polished substrates are much higher than those of T3 polished[40] samples, whatever the cleaning procedure.

The same task has been performed with BK7 substrates. Some results are given in Fig. 12. There is a contribution of the substrate bulk absorption that corresponds to an absorptance of approximately 40 ppm under our experimental conditions. From these results we can conclude the following:

(a) For commercial grade polished substrates, soft automatic cleaning leads to the best uniformity and generally to the lowest mean absorptance;

(b) For commercial grade polished substrates, ultrasonic cleaning leads to mean value and peak-to-peak variations of absorptance, both of which are higher than those obtained with soft automatic cleaning;

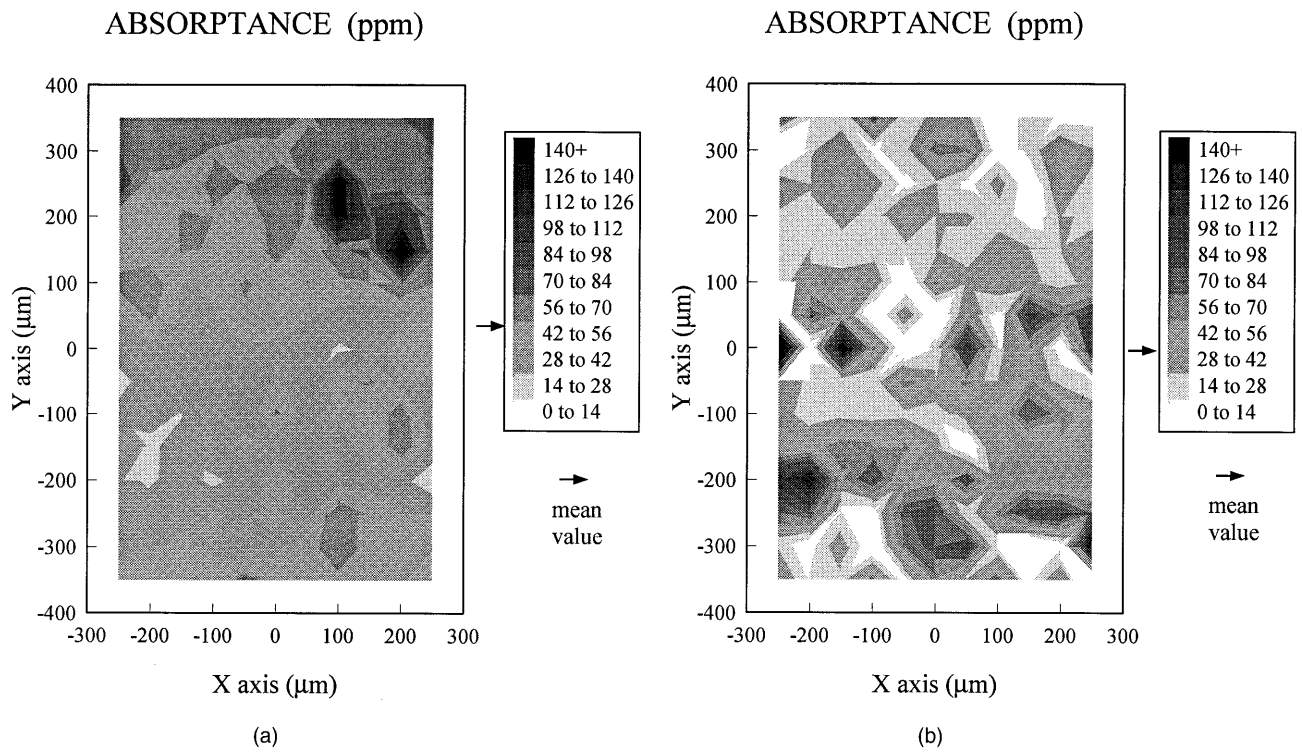

Fig. 10. Absorption mapping of the same area on a BK7 bare substrate (a) before, (b) after cleaning by the use of a conventional procedure through an automatic cleaning apparatus. The spatial distribution of absorption is completely modified, whereas the average surface absorptance decreases from 54 down to 40 ppm.

(c) On the other hand, the two cleaning procedures of T3 polished[40] substrates give similar results for both mean and maximum values.

We can see that the cleaning behavior of BK7 surfaces and their optical performances in terms of absorption are different from those of fused silica. These absorption data bear out results about physical and chemical properties of glass surfaces.

In Fig. 13 we give, in histogram form, the mean values of surface absorptance of 52 fused-silica and 31 BK7 substrates, all T3 polished[40] and cleaned with the same automatic procedure. The mean values of surface absorptance for fused-silica substrates range from 3 to 20 ppm. Those measured on BK7 substrates vary from 10 to 90 ppm. The average value is 7.9 ppm for the whole set of fused-silica substrates and 52 ppm for BK7 substrates. The behavior of these two kinds of surfaces in terms of optical absorp-

Table 3. Mean Surface Absorptance Values (ppm) before and after Cleaning for T3 Polished[40] Substrates

Substrate	Before Cleaning	After Cleaning	Ratio After/ Before (%)
BK7	60	45	75
	54	40	74
	60	54	90
	58	45	78
Fused silica	5.7	6.0	105
	6.1	5.2	85

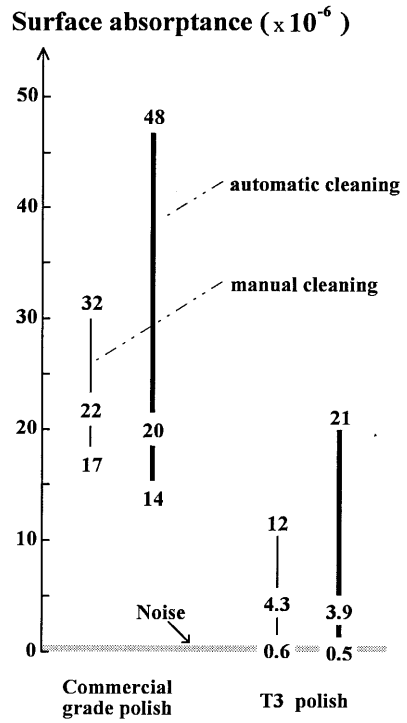

Fig. 11. Influence of polishing quality on minimum, mean, and maximum values of absorption. Example of results for two fused-silica substrates polished in different conditions and successively cleaned with increasingly effective cleaning procedures are given: soft manual cleaning (thin solid lines) then ultrasonic automatic cleaning (heavy solid lines). For each sample, measurements are performed on the same area.

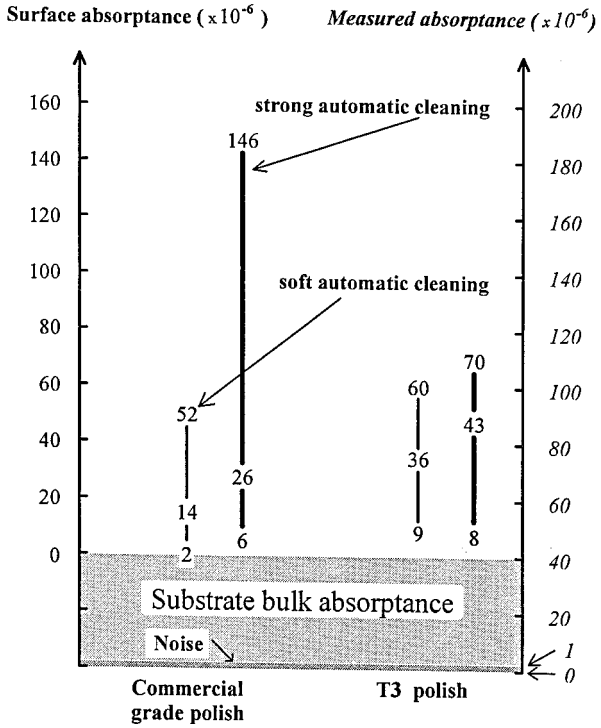

Fig. 12. Influence of polishing quality on minimum, mean, and maximum values of surface absorptance for two BK7 substrates polished under different conditions and successively cleaned with increasingly effective cleaning procedures: soft (thin solid lines) then ultrasonic (heavy solid lines) automatic cleaning. For each sample, measurements are performed on the same area.

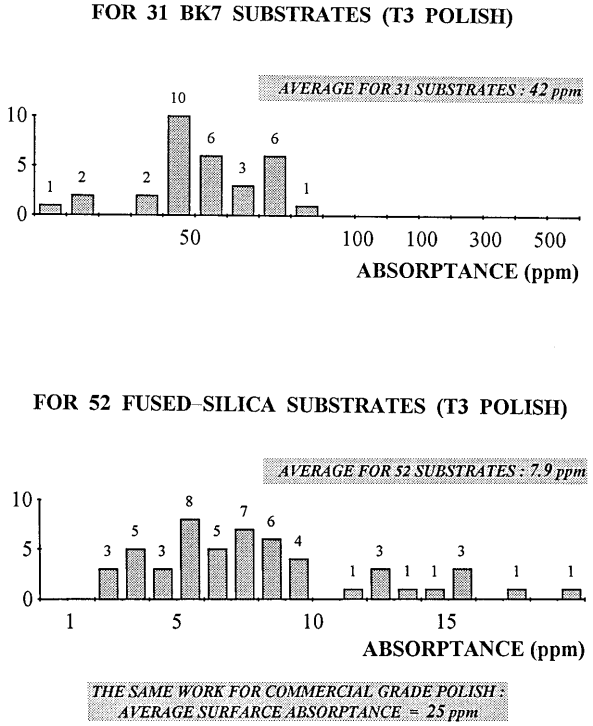

Fig. 13. Histogram of mean values of surface absorptance for 52 fused-silica substrates and 31 BK7 substrates, all T3 polished[40] and cleaned under the same conditions (ultrasonic automatic cleaning). Generally the defects of absorptance higher than some 100 ppm can be seen through a Nomarski microscope.

tion is different, even if their preparation procedures are similar.

Furthermore, the same results obtained with commercial grade polished substrates show that polishing procedures have a great influence on the surface absorption of bare substrates: two sets of the same fused-silica substrates lead to 7.9-ppm average absorptance for T3 polished[40] samples and to 25 ppm for commercial grade polished ones.

5. Conclusion

PD is a powerful tool for the characterization of optical coatings. We have presented three configurations used for implementing this technique. No configuration is better than the other ones. Each of them presents advantages and disadvantages, and they are complementary. They require the same equipment and the choice of one of them depends on the purpose of measurement (thermal parameter determination, absolute absorption measurement, spectroscopic measurement, high spatial resolution absorption mapping, or depth profiling of absorption) and also on experimental considerations (optical design and spectral properties of components and substrates to be characterized, wavelengths of the pump and probe beams). Generally speaking the transmission and the reflection configurations are well suited for absorption mapping with high spatial resolution, whereas the mirage effect is more convenient for thermal conductivity measurement.

Our theoretical and experimental study of calibration accuracy specifies the limits of PD with regard to the absolute absorption measurement. The accuracy of calibration can be evaluated at ~20%.

Photothermal absorption mapping has been shown to be a specific and complementary tool for the characterization of bare and coated substrates. Spatial variations of absorption are not necessarily associated with scattering variations and are not always visible through the Nomarski microscope. The study of bare substrates reveals the existence a nonuniform absorption localized at the surface. The surface absorptance is lower for very smooth surfaces, and multicomponent glasses have been shown to add significant complexity to surface behavior. Their surface absorptance is higher than that of monocomponent glasses such as fused silica. One can find further absorption data by PD on optical coatings in another paper.[44]

References and Notes

1. D. Ristau, X. C. Dang, and J. Ebert, "Interface and bulk absorption of oxyde layers and correlation to damage threshold at 1.064 μm," Nat. Bur. Stand. (U.S.) Spec. Publ. **727,** 298–312 (1984).
2. M. Rahe, E. Oertel, L. Reinhardt, D. Ristau, and H. Welling, "Absorption calorimetry and laser induced damage threshold measurements of AR-coated ZnSe and metal mirrors at 10.6 μm," in *Laser-Induced Damage in Optical Materials: 1990*,

H. E. Bennett, L. L. Chase, A. H. Guenther, B. Newman, and M. J. Soileau, eds., Proc. SPIE **1441,** 113–126 (1990).
3. R. Chow, S. Falabella, G. E. Loomis, F. Rainer, C. J. Stolz, and M. R. Kozlowski, "Absorption and damage thresholds of low-defect-density hafnia deposited with activated oxygen," in *Laser Induced Damage in Optical Materials: 1992*, H. E. Bennett, L. L. Chase, A. H. Guenther, B. Newman, and M. J. Soileau, eds., Proc. SPIE **1848,** 349–359 (1992).
4. M. R. Lange, J. K. MacIver, and A. H. Guenther, "Laser damage threshold predictions based on the effects of thermal and optical properties employing a spherical impurity model," Nat. Bur. Stand. (U.S.) Spec. Publ. **668,** 454–465 (1983).
5. S. M. J. Akhtar, D. Ristau, and J. Ebert, "Thermal conductivity of dielectric films and correlation to damage thresholds at 1064 nm," Natl. Inst. Stand. Technol. Spec. Publ. **752,** 345–351 (1986).
6. A. H. Guenther and J. K. MacIver, "The role of thermal conductivity in the pulsed laser damage sensitivity of optical thin films," Thin Solid Films **163,** 203–214 (1988).
7. A. C. Boccara, D. Fournier, W. Jackson, and N. M. Amer, "Sensitive photothermal deflection technique for measuring absorption in optically thin media," Opt. Lett. **5,** 377–379 (1980).
8. W. B. Jackson, N. M. Amer, A. C. Boccara, and D. Fournier, "Photothermal deflection spectroscopy and detection," Appl. Opt. **20,** 1333–1344 (1981).
9. M. A. Olmstead, N. M. Amer, S. Kohn, D. Fournier, and A. C. Boccara, "Photothermal displacement spectroscopy: an optical probe for solids and surfaces," Appl. Phys. A **32,** 141–154 (1983).
10. W. C. Mundy, R. S. Hughes, and C. K. Carniglia, "Photothermal deflection microscopy of dielectric thin films," Appl. Phys. Lett. **43,** 985–987 (1983).
11. J. A. Abate, A. W. Schmid, M. J. Guardalben, D. J. Smith, and S. D. Jacobs, "Characterization of micron-sized defects by photothermal deflection spectroscopy," Nat. Bur. Stand. (U.S.) Spec. Publ. **688,** 385–392 (1983).
12. M. Commandré, L. Bertrand, G. Albrand, and E. Pelletier, "Measurement of absorption losses of optical thin film components by photothermal deflection spectroscopy," in *Optical Components and Systems*, A. Masson, ed., Proc. SPIE **805,** 128–135 (1987).
13. M. Commandré and E. Pelletier, "Measurements of absorption losses in TiO_2 films by a collinear photothermal deflection technique," Appl. Opt. **29,** 4276–4283 (1990).
14. M. Commandré, P. Roche, G. Albrand, and E. Pelletier, "Photothermal deflection spectroscopy for the study of thin films and optical coatings: measurement of absorption losses and detection of photo-induced changes," in *Optical Thin Films and Applications*, R. Herrmann ed., Proc. SPIE **1270,** 82–93 (1990).
15. S. E. Watkins, R. Heimlich, R. Reis, "Mapping of absorption in optical coatings," in *Laser-Induced Damage in Optical Materials: 1991*, H. E. Bennett, L. L. Chase, A. H. Guenther, B. E. Newnam, and M. J. Soileau, eds., Proc. SPIE **1624,** 246–255 (1991).
16. Z. L. Wu, M. Reichling, E. Welsch, D. Schäfer, Z. X. Fan, and E. Matthias, "Defect characterisation for thin films through thermal wave detection," in *Laser-Induced Damage in Optical Materials: 1991*, H. E. Bennett, L. L. Chase, A. H. Guenther, B. E. Newnam, and M. J. Soileau, eds., Proc. SPIE **1624,** 271–281 (1991); M. Reichling, E. Welsch, A. Duparré, and E. Matthias, "Photothermal absorption microscopy of defects in ZrO_2 and MgF_2 single-layer films," Opt. Eng. **33,** 1334–1342 (1994).
17. Z. L. Wu, M. Reichling, H. Grönbeck, Z. X. Fan, D. Schaefer, and E. Matthias, "Photothermal measurement of thermal conductivity of optical coatings," in *Laser-Induced Damage in Optical Materials*, H. E. Bennett, L. L. Chase, A. H. Guenther, B. E. Newnam, and M. J. Soileau, eds., Proc. SPIE **1624,** 331–345 (1991), and references therein; M. Reichling and H. Grönbeck, "Harmonic heat flow in isotropic layered systems and its use for thin film thermal conductivity measurements," J. Appl. Phys. **75,** 1914–1922 (1994).
18. M. Commandré, "Caractérisation de l'absorption dans les composants optiques en couches minces par déflexion photothermique," Thèse de Doctorat d'Etat (Université d'Aix-Marseille, Marseille, 1992).
19. M. Commandré, P. Roche, J. P. Borgogno, and G. Albrand, "Surface contamination of bare substrates. Mapping of absorption and influence on deposited thin films," in *Optical Interference Coatings*, F. Abelès, ed., Proc. SPIE **2253,** 982–992 (1994).
20. M. Commandré, P. Roche, J. P. Borgogno, and G. Albrand, "Absorption mapping for characterization of glass surfaces," Appl. Opt. **34,** 2372–2379 (1995).
21. M. Commandré, P. Roche, J. P. Borgogno, and G. Albrand, "Effects of deposition conditions on thin film bulk and interface absorption," in *Optical Interference Coatings*, F. Abelès, ed., Proc. SPIE **2253,** 1253–1262 (1994).
22. P. Roche, M. Commandré, R. Mollenhauer, and F. Flory, "Interpretation of measurements of both losses on guided propagation and absorption from a model of absorbing transition layers," in *Optical Interference Coatings*, F. Abelès, ed., Proc. SPIE **2253,** 1286–1296 (1994).
23. C. Amra, M. Ranier, C. Grèzes-Besset, S. Maure, F. Cleva, R. Mollenhauer, and G. Albrand, "Loss anomalies in multilayer planar waveguides," in *Optical Interference Coatings*, F. Abelès, ed., Proc. SPIE **2253,** 1005–1020 (1994).
24. E. Welsch, "Absorption measurements," in *Thin Films for Optical Coatings*, R. E. Hummel and K. H. Guenther, eds. (CRC, Boca Raton, Fla., 1995), Chap. 9, pp. 243–272 and references therein.
25. M. Commandré and P. Roche, "Characterisation of absorption by photothermal deflection," in *Thin Films for Optical Systems*, F. Flory, ed. (Dekker, New York, 1995), Chap. 12, pp. 329–365.
26. E. Abraham and J. M. Halley, "Some calculations of temperature profiles in thin films with laser heating," Appl. Phys. A **42,** 279–285 (1987).
27. G. Rousset, F. Charbonnier, and F. Lepoutre, "Influence of radiative and convective transfers in a photothermal experiment," J. Appl. Phys. **56,** 2093–2096 (1984).
28. F. Flory, H. Rigneault, N. N. Maythaveekulchai, and F. Zamkotsian, "Characterization by guided wave of instabilities of optical coatings submitted to high-power flux: thermal and third-order nonlinear properties of dielectric thin films," Appl. Opt. **32,** 28, 5628–5639 (1993).
29. J. Opsal, A. Rosencwaig, and D. L. Willenborg, "Thermal wave detection and thin film thickness measurements with laser beam deflection," Appl. Opt. **22,** 3169–3176 (1983).
30. D. Ristau and J. Ebert, "Development of a thermographic laser calorimeter," Appl. Opt. **25,** 4571–4578 (1986).
31. D. L. Decker, L. G. Koshigoe, and E. J. Ashley, "Thermal properties of optical thin film materials," Nat. Bur. Stand. Spec. Publ. **727,** 291–297 (1984).
32. J. C. Lambropoulos, M. R. Joly, C. A. Amsden, S. E. Gilman, M. J. Sinicropi, D. Diakomihalis, and S. D. Jacobs, "Thermal conductivity of dielectric thin films," J. Appl. Phys. **66,** 4230–4242 (1989).
33. V. Scheuer, C. Schuchert, and T. Tschudi, "The influence of small amounts of impurities in sputtered laser mirrors on their performance," in *Thin Films in Optics*, T. T. Tschudi, ed., Proc. SPIE **1125,** 54–60 (1990).
34. P. Roche and E. Pelletier, "Characterisation of optical surfaces

by measurement of scattering distribution," Appl. Opt. **23,** 3561–3566 (1984).
35. P. A. Temple, "Examination of laser damage sites of transparent surfaces and films using total internal reflection microscopy," in *Laser Induced Damage in Optical Materials: 1979*, Nat. Bur. Stand. Spec. Publ. **568,** 333–341 (1979).
36. F. L. Williams, C. K. Carniglia, B. J. Pond, and W. K. Stowell, "Investigation of thin films using total internal reflection microscopy," in *Laser Induced Damage in Optical Materials: 1989*, Nat. Inst. Stand. Technol. Spec. Publ. **801,** 299–308 (1989).
37. R. C. Estier, N. S. Nogar, and R. A. Schmell, "The detection, removal and effect on damage thresholds of cerium impurities on fused silica," in *Laser Induced Damage in Optical Materials: 1988*, Nat. Inst. Stand. Technol. Spec. Publ. **775,** 183–188 (1988).
38. T. Raj, D. E. McCready, and C. K. Carniglia, "Substrate cleaning in vacuum by laser irradiation," in *Laser Induced Damage in Optical Materials: 1988*, Nat. Inst. Stand. Technol. Spec. Publ. **775,** 152–165 (1988).
39. R. S. Hockett, "Quantitative analysis of surface trace metal contamination on substrates and films by TXRF," in *Laser Induced Damage in Optical Materials: 1989*, Nat. Inst. Stand. Technol. Spec. Publ. **801,** 239–253 (1989).
40. Very smooth surface finish (French Standard NF S 10-006). The rms roughness is ~0.3 nm.
41. H. K. Pulker, "Nature of a surface," in *Coating on Glass* (Elsevier, New York, 1984), Chap 3, pp. 34–42.
42. T. S. Izumitani, *Optical Glass*, American Institute of Physics Translation Series (American Institute of Physics, New York, 1986), Chap. 2, pp. 15–55.
43. K. Kinosita, "Surface deterioration of optical glasses," in *Progress in Optics*, E. Wolf, ed. (North-Holland, Amsterdam, 1965), Vol. 4, pp. 85–143.
44. P. Roche, M. Commandré, L. Escoubas, J. P. Borgogno, G. Albrand, and B. Lazarides, "Substrate effects on absorption of coated surfaces," Appl. Opt. **35,** 5059–5066 (1996).